Charging and discharging processes of carbon nanotubes probed by electrostatic force microscopy

M. Zdrojek[a)]
Institut d'Electronique, de Microélectronique et de Nanotechnologie, CNRS UMR 8520, Dpt ISEN, Avenue Poincaré, F-59652 Villeneuve d'Ascq, France and Faculty of Physics, Warsaw University of Technology, Koszykowa 75, 00-662 Warsaw, Poland

T. Mélin, H. Diesinger, and D. Stiévenard
Institut d'Electronique, de Microélectronique et de Nanotechnologie, CNRS UMR 8520, Dpt ISEN, Avenue Poincaré, F-59652 Villeneuve d'Ascq, France

W. Gebicki and L. Adamowicz
Faculty of Physics, Warsaw University of Technology, Koszykowa 75, 00-662 Warsaw, Poland

(Received 7 August 2006; accepted 20 September 2006; published online 14 December 2006)

Electrostatic properties of individually separated single-walled carbon nanotubes (SWCNTs), double-walled carbon nanotubes (DWCNTs), and multiwalled carbon nanotubes (MWCNTs) deposited on insulating layers have been investigated by charge injection and electric force microscopy (EFM) experiments. Delocalized charge patterns are observed along the CNTs upon local injection from the EFM tip, corresponding to (i) charge storage in the nanotubes and to (ii) charge trapping in the oxide layer along the nanotubes. The two effects are dissociated easily for CNTs showing abrupt discharge processes in which the charge stored in the CNT are field emitted back to the EFM tip, while trapped oxide charge can subsequently be imaged by EFM, clearly revealing field-enhancement patterns at the CNT caps. The case of continuous discharge processes of SWCNTs, DWCNTs, and MWCNTs is discussed, as well as the evolution of the discharge time constants with respect to the nanotube diameter. © *2006 American Institute of Physics*.
[DOI: 10.1063/1.2392674]

I. INTRODUCTION

The understanding of the electronic behavior of charged carbon nanotubes (CNTs) and of CNTs in a charged environment is a crucial issue in electronic applications such as field-effect transistors or CNT-based nanoelectromechanical devices. Electrostatic force microscopy appears as a dedicated tool to map and study the spatial distributions of electric field and charges at the nanometer scale, but up to now only few studies have applied this technique to carbon nanotubes. For instance, it has been found that CNTs can exhibit a potential barrier leading to charge trapping in CNT loops on insulating surface,[1] confirming the importance of substrate charges around the CNTs in the operation of electronic devices.[2] Up to now, electrostatic imaging[3,4] and charging issues[5,6] have been studied mainly in the case of single-walled carbon nanotubes (SWCNTs). One experimental work[7] has so far been published on the charging properties of multiwalled carbon nanotubes.

We present in this paper an extensive discussion about charging effects in carbon nanotubes deposited on oxide (SiO_2) layers. The article is organized as follows. We first describe the sample preparation and experimental procedures used for charge injection and detection and characterize both the local charge injection in SiO_2 layers and the delocalized charge patterns observed in the case of CNTs. In a second part, we focus on CNTs exhibiting abrupt discharging at nanotube defect points or at the nanotube caps. These field-emission effects enable to easily identify charge storage *in the nanotube* versus charge storage *in the oxide layer along the nanotubes*. The field-enhanced charge emission patterns from CNT caps are also analyzed as a function of the CNT cap diameter. In the last part we comment on discharging processes which are not related to abrupt discharging effects of the nanotubes. The continuous discharging of SWCNTs, double-walled carbon nanotubes (DWCNTs), and multiwalled carbon nanotubes (MWCNTs) is discussed, as well as the evolution of the discharge time constants with respect to the nanotube diameter.

II. SAMPLES AND EXPERIMENTS

A. Samples

Purified SWCNTs, DWCNTs, and MWCNTs grown by catalytic carbon vapor deposition[8] were obtained commercially from Nanocyl (Belgium). As-bought nanotubes were placed in dichloromethane solutions, separated by low-power ultrasonication, and finally dispersed by spin coating onto substrates, with a tunable CNT density in the range of 1–10 per μm^2. Electrostatic experiments have been performed using doped silicon substrates covered with a 200 nm thermally grown insulating SiO_2 layer. Before the CNT deposition, arrays of metal markers have been fabricated using electron beam lithography in order to localize individual nanotubes on surfaces and consist in 30 nm thick platinum squares of 500×500 nm^2 size separated by a 5 μm pitch.

a)Electronic mail: zdrojek@if.pw.edu.pl

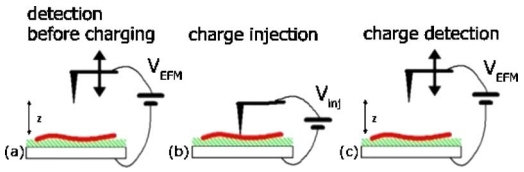

FIG. 1. (Color online) Schematics of the charge injection and EFM detection experiments. (Left) EFM data acquisition before charge injection. The recorded EFM signal is the cantilever resonance frequency shift when the tip is biased at V_{EFM} and scanned at a constant distance z above the sample; (middle) charge injection with the tip in contact with the nanotube and biased at V_{inj} with respect to the substrate; (right) EFM data acquisition after injection.

B. Experimental procedure

Charge injection and detection experiments have been operated on a Multimode/Nanoscope IIIA atomic force microscope (Veeco Instruments) at room temperature. The microscope was placed under a dry nitrogen atmosphere in order to avoid (i) charge leakage due to adsorbed surface water and (ii) anodic oxidation during the charge injection experiments. Commercial Pt–Ir coated cantilevers with ~60 kHz resonance frequency and 1–3 N/m spring constants have been used.

Charging experiments have been achieved by first localizing individual CNTs from the sample topography acquired in intermittent contact mode atomic force microscopy (AFM). Charges are then injected[9] in a given nanotube using local approach-retract curves with the electric force microscopy (EFM) cantilever biased at the injection voltage V_{inj} (typically $V_{inj}=-2$ V up to -12 V) with respect to the sample silicon substrate. In this process, the distance z between the biased EFM tip and the substrate is periodically swept (1 Hz sweep rate), and its minimum value is tuned in order to reach a *permanent contact regime* between the EFM tip and the CNT during the z sweep, in which the cantilever oscillation amplitude is nullified and a cantilever quasistatic deflection is monitored. This enables to adjust the tip-CNT contact force (here a few nanonewtons, as measured from the cantilever static deflection) and the contact duration (typically 100 ms for tip-substrate distance sweeps with 1 s period). Charging times given in this paper (1–4 min) always refer to the total duration of the approach-retract sweeps, while the cumulated duration of the permanent contacts between the EFM tip and the CNT during the approach-retract sweeps typically corresponds to one tenth of the charging times.

Topography and EFM images are acquired simultaneously in an interleave scheme. For each sample scan line, the topography is first acquired in intermittent contact mode with the tip bias set to zero. EFM data are then recorded in a second pass [see Fig. 1(a)] in which the cantilever is moved at a distance z parallel to the substrate plane (usually $z=70-100$ nm, as measured between the tip apex and the substrate). During this linear pass at constant height with respect to the substrate plane, the EFM cantilever is mechanically oscillating around its z position and with a frequency close to its resonance frequency f_0 and biased at the detection bias V_{EFM} with respect to the substrate. Recorded EFM data consist of the cantilever frequency shift Δf induced by electrostatic force gradients. In absence of charge, the frequency shift Δf is due to the increase of the tip-substrate capacitance during the linear pass of the tip over the CNT and is thus a capacitive signal induced by the presence of nanotube deposited on the surface. Since capacitive forces are attractive and proportional to $(V_{EFM})^2$, the corresponding EFM signal is a negative frequency shift,[10] irrespective of the sign of V_{EFM}: uncharged CNTs are hence always imaged as dark features in EFM images. This, however, no longer holds when the CNTs are charged, because the total electric force also includes a component proportional to the nanotube charge Q and to V_{EFM}.[10] In our experiments, the nanotubes are negatively charged ($V_{inj}<0$), and we used negative V_{EFM} values for charge detection ($V_{EFM}=-2$ or -3 V). Consequently, the additional force component is repulsive and leads to a positive frequency shift imaged as a bright feature in EFM images. Charge and capacitive force gradients, however, compete with each other, so even for $V_{EFM}\times V_{inj}>0$, charged nanotubes can only be imaged as bright features provided that charge signals predominate over capacitive EFM signals. Such imaging conditions can be reached either for sufficiently charged CNTs, or by lowering the detection bias V_{EFM}. These scanning conditions have been used for all EFM images reported in this article, so that dark and bright features in EFM images will always correspond here to capacitive and charge effects, respectively. Finally, in practice, reference EFM images of the CNTs are always acquired prior to charging experiments as depicted in Fig. 1(a), so as to check the CNT electrostatic state before charging. Charge injection is then performed [Fig. 1(b)] as described above, and the EFM image is finally recorded after charge injection [Fig. 1(c)].

C. Oxide charging

We first characterize the 200 nm thick thermal oxide layers used in this work, which will be later used for comparison with charge injection experiments performed on CNTs. An EFM scan before charging is shown in Fig. 2(a) (10 Hz color scale) and displays no capacitive feature since the SiO_2 surface is flat. After injection (here with a tip biased at $V_{inj}=-5$ V during 2 min), the EFM scan [Fig. 2(b), 10 Hz color scale] exhibits a bright circular spot of maximum positive frequency shift ~7.5 Hz at the injection point. At a fixed elapsed time t after charge injection, the EFM charge signal is analyzed using a two-dimensional spatial Gaussian distribution law $\Delta f=A/(2\pi\sigma^2)\exp-[r^2/2\sigma^2]$, where r accounts for surface coordinates, A (in Hz nm^2) is the surface integral of the EFM charge signal, and σ^2 (in nm^2) is the squared standard deviation of the charge distribution. A and σ^2 are thus adjustable parameters which vary as a function of t. The diffusion coefficient D of surface charges can be simply obtained by $\sigma^2-\sigma^2(t=0)=2Dt$.

The evolution of the fitted parameters A and σ^2 with t is shown in Fig. 2(c). The surface charge is found to weakly diffuse in the oxide surface with a diffusion coefficient $D\sim(20\text{ nm})^2/\text{min}$ measured from a linear fit of σ^2 as a function of time. The EFM signal integral A is also found to slightly decrease within the 25 min time scale of Fig. 2(c). At

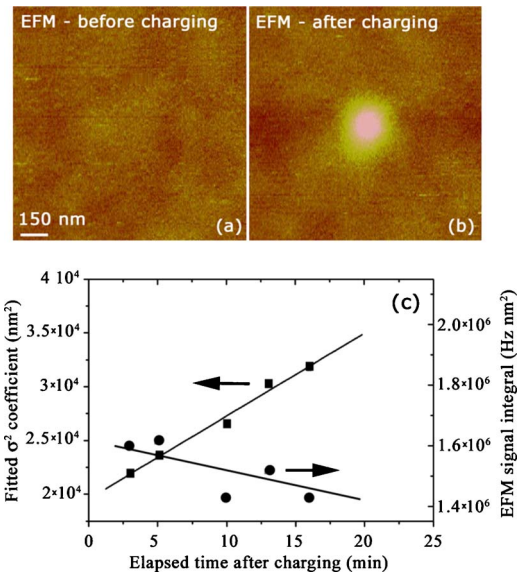

FIG. 2. (Color online) (a) EFM image (10 Hz color scale, $V_{EFM}=-3$ V) of a 200 nm thick thermally grown silicon dioxide layer. Since the sample surface is almost flat, no capacitive feature can be seen here. (b) EFM image acquired after a local charge injection ($V_{inj}=-5$ V for 2 min). The bright circular feature corresponds to a maximum frequency shift $\Delta f \sim +7.5$ Hz. (c) Analysis of the EFM charge signal integral amplitude (circles) and of the EFM charge signal width, as measured from the squared standard deviation σ^2 (squares) in a Gaussian distribution model.

a larger time scale, almost exponential decays can be observed, with typical decay times of the order of ~40 min.

D. CNT charging

First we present charging experiments performed on a 19 nm diameter multiwalled nanotube [topography image in Fig. 3(a)]. The EFM image acquired with $V_{EFM}=-3$ V before charge injection is shown in Fig. 3(b) and reveals a dark feature corresponding to the capacitive footprint of the uncharged nanotube. Charge injection was made using $V_{inj}=-5$ V during 2 min at the injection point indicated by the arrow in Fig. 3(a). The delocalization of the injected charge along the MWCNT is visible from the EFM image of Fig. 3(c) (taken after the injection) in which the nanotube is homogeneously bright (positive frequency shift) as a result of the dominant repulsive interaction between the MWCNT negative charge and the negative charge at the biased tip apex. The delocalization of the injected charge over microns along the CNTs is consistent with previous results.[5,6] From preliminary numerical calculations of the MWCNT charge densities from EFM signals, we estimate the linear charge density to be here $\sim 160|e|/\mu$m, lower[6] than the value expected from a charging of the CNT-substrate capacitance. The detailed and quantitative analysis of the CNT charge densities will, however, fall beyond the scope of this paper.

The cross sections of EFM signals are displayed in Fig. 3(d) and have been taken at the CNT position indicated by

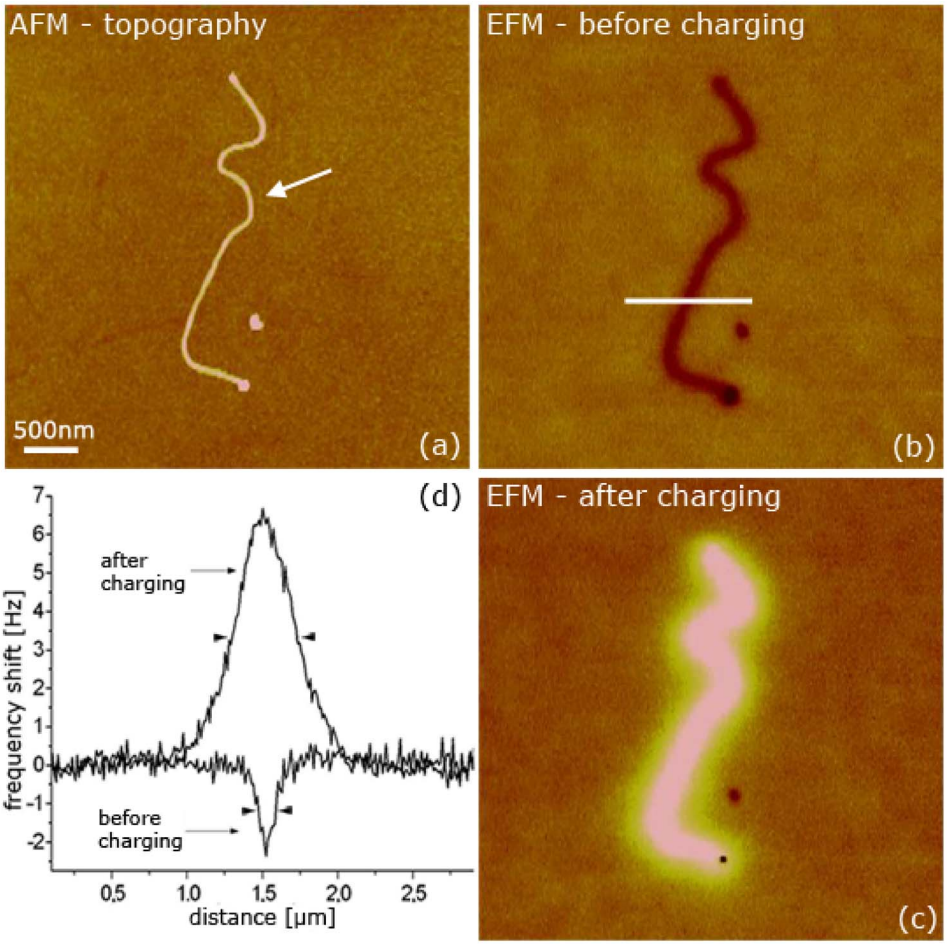

FIG. 3. (Color online) (a) Atomic force microscopy image of MWNT of ~19 nm diameter on a 200 nm silicon dioxide surface. (b) EFM image ($V_{EFM}=-3$ V) acquired before charging (10 Hz color scale) with a tip-substrate distance $z \sim 100$ nm. (c) EFM image taken in the same conditions, after a charge injection performed at the point indicated by an arrow in (a), using $V_{inj}=-5$ V for 2 min. (d) Cross sections of the EFM scans for the cases (b) and (c). The position of the cross section is shown by the horizontal bar in (b). The full width at half minimum (FWHM) of the EFM signals before and after charging (respectively, ~100 and 440 nm) is marked by the triangles as a guide to the eye.

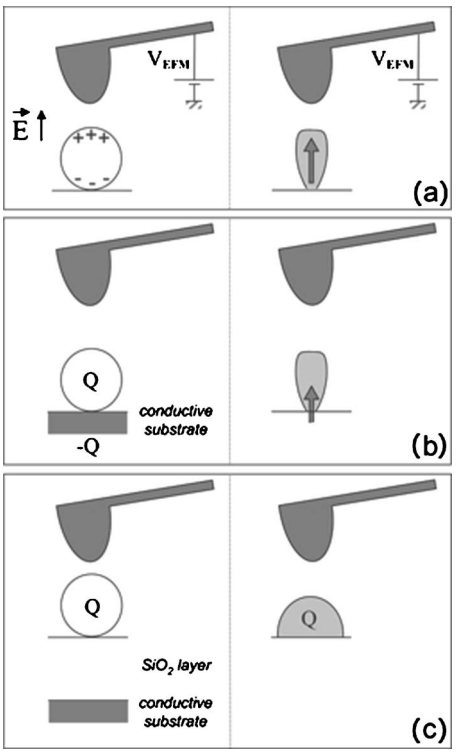

FIG. 4. (a) (Left) Cross-section schematics of a neutral CNT placed in the electric field created by the EFM tip biased at V_{EFM}. The polarized CNT is detected as a surface dipole (right). (b) (Left) Schematics of the charge detection for a CNT on a conductive substrate. The CNT charge is screened by its electrostatic image with respect to the substrate and is detected (right) as a surface dipole. (c) Similar schematics when the charged CNT is on an insulating layer and detected (right) as a surface charge. The charge field is here much more isotropic than the CNT polarization field in (a), which accounts for the different widths of the EFM signals of the uncharged and charged CNT in Figs. 3(b) and 3(c), respectively.

the horizontal bar in Fig. 3(b). The full width at half minimum (FWHM) of the EFM signal of the uncharged nanotube equals ~100 nm and is already larger than the apparent CNT diameter in the topography image, as can be seen from the EFM images in Figs. 3(a) and 3(b). This simply illustrates the lower spatial resolution of EFM compared to topography measurements, which is due to the long range of electrostatic forces and the large (80–100 nm) tip-surface distance during EFM data acquisition. A more striking feature is the broadening of the EFM signals when the nanotube is charged (440 nm FWHM), as seen from Fig. 3(d) and from the comparison between Figs. 3(b) and 3(c). This effect does not occur in EFM experiments performed in nanostructures deposited on conductors,[11] where the width of EFM signals remains unchanged after charging.

The two situations can be explained by the difference in the electrostatic screening induced by the substrate supporting the nanostructures, as illustrated in Fig. 4. Whatever the nature of the substrate supporting the nanostructure, the EFM capacitive signal stems from the polarization of the nanostructure in the electric field induced by the EFM tip and thus corresponds to an effective dipole oriented perpendicular to the surface, as illustrated in Fig. 4(a). The EFM charge signal, however, strongly depends on the nature of the host substrate. When nanostructures are deposited on conductors, stored charges are screened by substrate image charges and also behave as surface dipoles oriented perpendicular to the surface[11] as sketched in Fig. 4(b). In this situation, both charge and capacitive EFM signals consequently display similar variations, and thus identical FWHMs as observed in Ref. 11. In contrast, the use of a 200 nm thick SiO_2 layer on the substrate makes the ~100 nm tip-nanostructure distance fairly smaller than the 400 nm separation between the nanostructure charge and its electrostatic image with respect to the substrate. In that case, the nanostructure charge is not screened by the conductive substrate at first order and thus behaves like a charge rather than a dipole [see Fig. 4(c)]. As a result, the nanostructure charge signal is expected to be much more isotropic than the capacitive signal. This effect accounts for the bigger FWHM of the CNT charge signal [EFM image of Fig. 3(c)] compared to the CNT capacitive signal [EFM image of Fig. 3(b)]. Finally the change observed experimentally in the FWHM of the CNT EFM signal upon charging is a demonstration of the neutral character of the nanotube after its deposition on the silicon dioxide surface and prior to charging experiments, in contrast with experiments performed on conductive substrates, where charge can be transferred between the substrate and the CNTs.[17] The upper bound of the charge densities prior to charge injection can be obtained from Fig. 3(d). As seen previously, the narrow FWHM of the EFM signal prior to charging indicates that the CNT is almost neutral, as compared with the larger FWHM of the EFM signal measured after charging. More quantitatively, we estimate that the CNT charge—if any—before charge injection experiments corresponds to an EFM signal less than 0.5 Hz, and thus to a maximum $|10\ e/\mu m|$ linear charge density.

III. ABRUPT DISCHARGE PROCESSES IN CARBON NANOTUBES

In this section, we review the phenomena associated with abrupt discharge processes in carbon nanotubes. First, we discuss discharging at single/multiple points along the CNT and at the CNT caps, which unambiguously demonstrate charge storage *in* carbon nanotubes. Then, we report on the field emission of charges to the oxide layer supporting the CNTs and its enhancement at the CNT caps.

A. Abrupt discharges at single and multiple defects

A sudden discharge behavior of the charge injected in a MWCNT is presented in Fig. 5. In Fig. 5(a) the topography of a MWCNT with ~18 nm diameter and ~2.3 μm length is shown. The point used for charge injection experiments is indicated by the arrow. The EFM signal before charging [Fig. 5(b)] shows a negative frequency shift equal to 1.2 Hz. After the injection (V_{inj}=−6 during 3 min) the EFM scan is started from the bottom to the top [Fig. 5(c)]. The nanotube appears first as homogeneously charged (bright feature with maximum frequency shift +8.2 Hz), but then undergoes three abrupt discharges at the points labeled d1, d2, and d3, each discharge occurring within one scan line. The CNT EFM image was then found stable upon further scanning (no more sudden discharges), indicating that the bright halo surround-

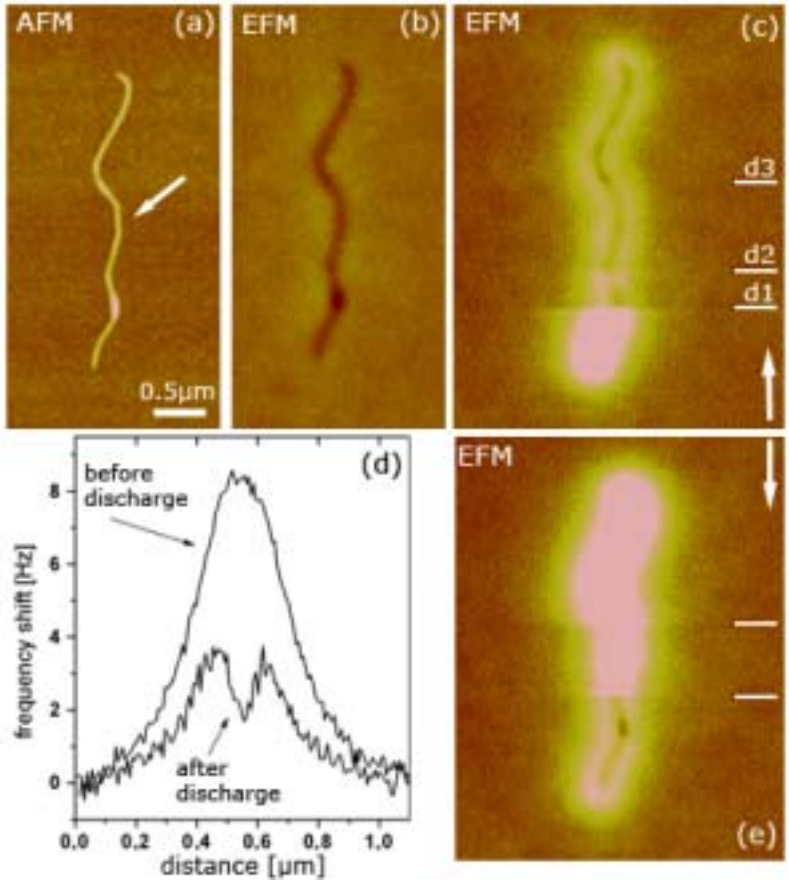

FIG. 5. (Color online) (a) AFM topography picture of ~2.3 μm long MWCNT with ~18 nm diameter. (b) EFM image acquired before charging. The capacitive footprint of the nanotube topography is visible and corresponds to 1.2 Hz negative frequency shift. (c) EFM scan after charge injection with the tip biased at V_{inj} =−6 V for 3 min at the injection point indicated in (a). The direction of data acquisition is depicted by the vertical arrow. Three discharge points (d1, d2, and d3 labeled in the figure) successively occur during the CNT scanning. After the discharge, the CNT capacitive footprint is clearly visible in the EFM image, however, surrounded by a bright halo. This EFM image proved stable upon further scanning. (d) EFM signal taken across the CNT before and after the sudden discharge labeled d1 in (c). (e) EFM scan after injection with the tip biased at V_{inj}=−7 V. The image is scanned from top to the bottom (see vertical arrow). The two abrupt frequency shift drops which are visible in this scan correspond to the position of the discharges labeled d3 and d2 in (c).

ing the CNT capacitive footprint after the third discharge in Fig. 5(c) is due to charge emitted by the CNT and trapped in the oxide surface.[7] This effect will be discussed in the following. The CNT frequency shifts before and after d1 are compared in Fig. 5(d) and show that the capacitive footprint of the CNT topography can be already clearly identified after the first discharge while the EFM signal was dominated by the CNT charge just after injection.

To associate the discharge locations as specific nanotube points, an injection experiment has been made again at the same nanotube point using V_{inj}=−7 V. The resulting EFM image scanned from top to bottom is shown in Fig. 5(e) and was acquired ~2 h after the scan in Fig. 5(c). Two abrupt discharges are evidenced in Fig. 5(e) and correspond to the discharge points labeled d3 and d2 in Fig. 5(c). This demonstrates that abrupt discharges are induced by specific points along the MWCNT. At the discharge points, the CNT charge is field emitted back to the EFM tip apex which is grounded and intermittently brought into contact with the CNTs during the topography pass. The fact that the discharge occurs during topography imaging will be demonstrated in the next section. Abrupt discharges were observed mainly for MWCNTs with diameter smaller than 25 nm, with a maximum density of discharge points of a few μm^{-1} in case of multiple discharges.

We assume that the sudden discharge points are related to nanotube defects, such as vacancies and openings in the outer shells, or to metallic catalysts which can remain present inside the nanotube. The presence of defects in the investigated nanotubes has been confirmed by high resolution transmission electron microscopy (HRTEM) studies.[7] Combined EFM and HRTEM experiments would, however, be required to clearly relate the abrupt discharge points to the CNT structural properties.

B. Abrupt discharges at the CNT caps

Two examples of sudden discharges at MWCNT caps are evidenced, in the case of an individual MWCNT [Figs. 6(a) and 6(b)] and for a MWCNT network [Figs. 6(c) and 6(d)]. In both cases, the MWCNTs have been charged using V_{inj}=−5 V for 2 min and EFM images acquired from top to bottom. The nanotubes are first observed as negatively charged [bright features in Figs. 6(b) and 6(d)]. In both cases, the MWCNT sudden discharge is seen to occur when the tip gets in intermittent contact with the CNT during the topography scan: discharges in Figs. 6(b) and 6(d) are correlated with the CNT appearance in the topography scans of Figs. 6(a) and 6(c). This demonstrates that the nanotubes are discharged during topography scanning, but not during the EFM data acquisition. Hence, the CNT caps act as efficient discharging points, thus supporting our claim that the abrupt discharge is based on a field-emission process, in which the grounded EFM tip acts as counterelectrode. After the discharge, the nanotubes also exhibit a bright halo as after the discharge in Figs. 5(c) and 5(e), indicating the presence of residual negative charge, which will be discussed in the next section.

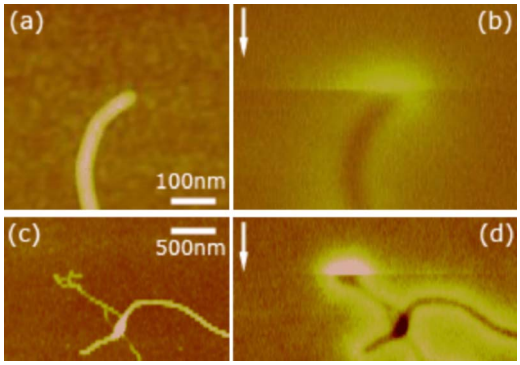

FIG. 6. (Color online) (a) AFM topography image of one end of MWCNT with length 1.6 μm and diameter ~21 nm. (b) EFM scan after a charge injection experiment using $V_{inj}=-5$ V for 2 min. The image is scanned from the top to the bottom as indicated by the arrow. A sudden discharge appears directly at the nanotube cap (4.5 Hz frequency drop). (c) AFM topography image of a part of a MWCNT network (total length >15 μm; diameter at the upper CNT cap ~10 nm). The pixels visible in the topography image are due to a low resolution data acquisition. (d) EFM scan after charge injection with the tip biased at $V_{inj}=-5$ V. The scan direction is indicated by the arrow. An abrupt discharge is visible at the upper part of the nanotube network.

C. Residual charge emission along CNTs

The EFM images of Figs. 5(c) and 5(e) (after discharge) and of Figs. 6(b) and 6(d) (after discharge at the CNT caps) all display a residual negative charge along the nanotube in the form of a bright halo around the nanotubes. The observation of the halo is due to the different FWHMs of charge and capacitive effects as pointed out in Sec. II D and to the imaging conditions used in this work ($V_{inj} \times V_{EFM} > 0$). The actual issue is to determine whether this negative charge corresponds to electrons still stored *in* the CNT, or to charge emitted by the CNT and trapped on the oxide surface. If not discussed, the issue of surface charge emission can lead to controversial interpretations of EFM images.[5,6] In Figs. 5 and 6, the bright halos observed after charging can be unambiguously attributed to charges trapped on the oxide surface for the following reasons: (i) the residual charge pattern cannot be removed by discharging the nanotube (i.e., performing a charge injection experiment on the CNT using $V_{inj}=0$ V); (ii) the residual charge pattern decays very slowly with time (at least a few hours) so that no evolution can be observed in the first subsequent EFM images acquired after the abrupt discharge phenomena. This behavior strongly contrasts with that of charge injected *in* the CNTs, which can be either removed by a local charge injection using $V_{inj}=0$ V, or abruptly emitted back to the EFM tip as described in the previous section. We finally would like to comment on the decay times of oxide charges stored in the vicinity of the nanotubes, which are found to be much larger than decay times on the bare oxide (~40 min, as seen from Sec. II C). The decay of charge injected in bare thin oxide layers has been proposed to result from the attraction between the oxide charge and their substrate images,[12] leading to a gradual move of oxide charges towards the conductive substrate electrode. In our case, the oxide charge near the CNTs is also subjected to an attractive image force from the CNTs themselves. This attractive interaction is consistent with the much longer retention times observed for oxide charge along the CNTs.

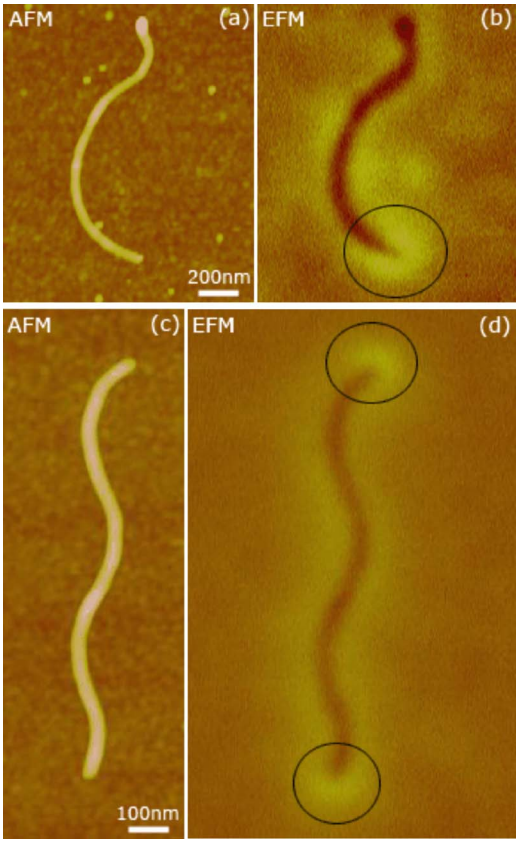

FIG. 7. (Color online) (a) AFM topography of MWCNT with two different cap diameters (11 and 27 nm for the lower and the upper caps, respectively). (b) Residual charge emission pattern after a charging experiment ($V_{inj}=-6$ V for 3 min). The smaller-diameter cap exhibits an enhanced charge emission (+2.5 Hz frequency shift; see dark circle), while no significant emission is observed in the vicinity of the upper cap. The frequency scale of the EFM image is 10 Hz. (c) Topography image of a 21 nm diameter MWCNT (d) EFM image (20 Hz frequency scale) after charge injection ($V_{inj}=-5$ V during 2 min) and the MWCNT discharge. It shows an enhanced charge emission near both caps (+3 Hz; see dark circles) in comparison with the charge emitted along the nanotube (+1.4 Hz frequency shift).

D. Enhanced charge emission at the CNT caps

We now report on the charge emission from the nanotube caps. Two examples are shown in Fig. 7. Figure 7(a) shows the topography of a MWCNT with different cap diameters (11 and 27 nm for the lower and upper cap, respectively). The EFM image of the residual charge emission pattern observed after charge and discharge is given in Fig. 7(b) and shows an enhanced charge emission at the smaller cap diameter. In contrast, no significant emission is observed in the vicinity of the upper cap, even upon injection at higher bias and with longer injection times.[13] Another MWCNT with a constant ~21 nm diameter is presented in Fig. 7(c) and shows an enhanced charge emission near both caps (+3 Hz) in comparison with the charge emitted along the nanotube (+1.4 Hz frequency shift).

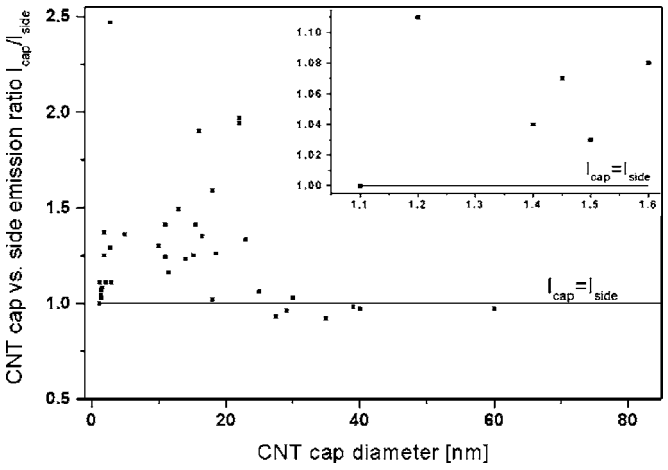

FIG. 8. Comparison between the charge emission from the CNT cap and from the CNT side. The plot has been obtained using ~40 caps of single, double and multiwalled CNTs. It displays the ratio I_{cap}/I_{side} of the emitted charge intensities at the CNT cap compared to the CNT side, as a function of the CNT cap diameter. The inset shows a zoom of the data for SWCNTs with diameter <1.6 nm.

It is known that the field enhancement at the CNT caps depends on the cap shape[14,15] and on the diameter of the nanotube. It is also considered that MWCNTs have different electron emission parameters than SWCNTs.[16] To test this dependence in our experiments, we plotted in Fig. 8 the ratio I_{cap}/I_{side} as a function of the CNT cap diameter, where I_{cap} is the intensity of the charge emission at the CNT cap and I_{side} is the intensity of the charge emission at the CNT side. Intensities of charge emission have been taken as proportional to the corresponding EFM frequency shifts. 40 CNT caps have been used in Fig. 8. In agreement with our previously published data[7] we do not observe a significant enhancement of electron emission for caps bigger than ~25 nm, i.e., $I_{cap}/I_{side}\sim 1$. An enhancement $(1<I_{cap}/I_{side}<2.5)$ is then visible for MWCNTs with diameter <25 nm, but the ratio I_{cap}/I_{side} displays strong fluctuations from one MWCNT to the other. We ascribe this phenomenon to the varied cap structures of the CNTs, which can be, for instance, either closed or open, as confirmed by transmission electron microscopy experiments.[7] Finally, no further emission enhancement can be observed for smaller diameter (<1.6 nm) nanotubes. This is especially visible for SWCNTs with diameters in the range of 1.1–1.6 nm for which the ratio I_{cap}/I_{side} only slightly stays above unity as seen in the inset of Fig. 8. This peculiarity may be related to the specific sample geometry used in our experiments, compared to usual field-emission setups. The sample substrate which plays the role of the collecting anode is here parallel to the CNTs. Thus, field lines stemming from the CNT caps are curved towards the substrate. Charge emitted from smaller CNT caps are hence emitted close to the CNTs and can consequently take part in the CNT charging mechanisms. This may drastically limit the accumulation of oxide charge close to CNT caps and account for the ratio I_{cap}/I_{side} close to unity for SWCNTs.

IV. CONTINUOUS DISCHARGE OF CNTS

We discuss in this section discharging phenomena which are not related with abrupt discharging processes. We present continuous discharging of SWCNTs, DWCNTs, and MWCNTs and comment on the evolution of the discharge time constants with respect to the nanotube diameter.

A. Continuous fast discharge of SWNTs and DWNTs

Charging experiments are presented in Fig. 9 for a SWCNT with 1 nm diameter. The white squares visible on this image are 500×500 nm^2 metal markers prepared by *e*-beam lithography and used for the nanotube localization. The EFM scan before injection ($V_{EFM}=-3$ V) is shown in Fig. 9(b). The nanotube and metal markers appear here as dark features, corresponding to uncharged objects. The EFM scan after injection ($V_{inj}=-5$ V during 3 min) is displayed in Fig. 9(c) and shows the delocalization of the injected charge along the whole SWCNT length (~30 μm), while the square metal markers remain uncharged. However, no abrupt discharge occurs in Fig. 9(c). As a consequence, one cannot here estimate directly the amount of charge stored *in the CNT* and the amount of charge trapped *on the oxide surface*, in contrast with CNTs exhibiting abrupt discharge phenomena as shown in Sec. III. To circumvent this, the CNT has been continuously scanned, and the two first images follow-

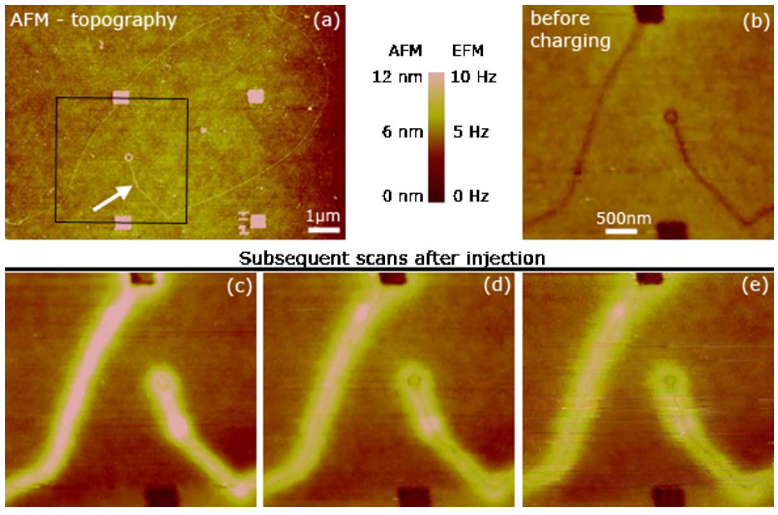

FIG. 9. (Color online) (a) AFM topography image of a SWCNT with 1 nm diameter. 500×500 nm^2 metal squares separated by a 5 μm pitch are visible in the image. One of the apexes of the SWCNT appears to be ring shaped. The length of the nanotube is ~32 μm. The arrow indicates the point used for charge injection experiments. (b) EFM image of the area indicated by the black square in (a), acquired before injection ($V_{EFM}=-3$ V). (Inset) Color scale bar for the AFM topography image and EFM scans. (c) EFM scan after a charge injection experiment with $V_{inj}=-5$ V for 3 min. The delocalization of the charge along whole nanotube is visible. A bright spot can also be seen at the injection point, showing that charges were also injected locally into the dielectric surface. [(d) and (e)] Successive EFM scans acquired after the injection shown in (c). The SWCNT discharge is visible by comparison of (c) with (or to) (d), while no further discharge is observable afterwards, as seen by comparison of (d) to (e).

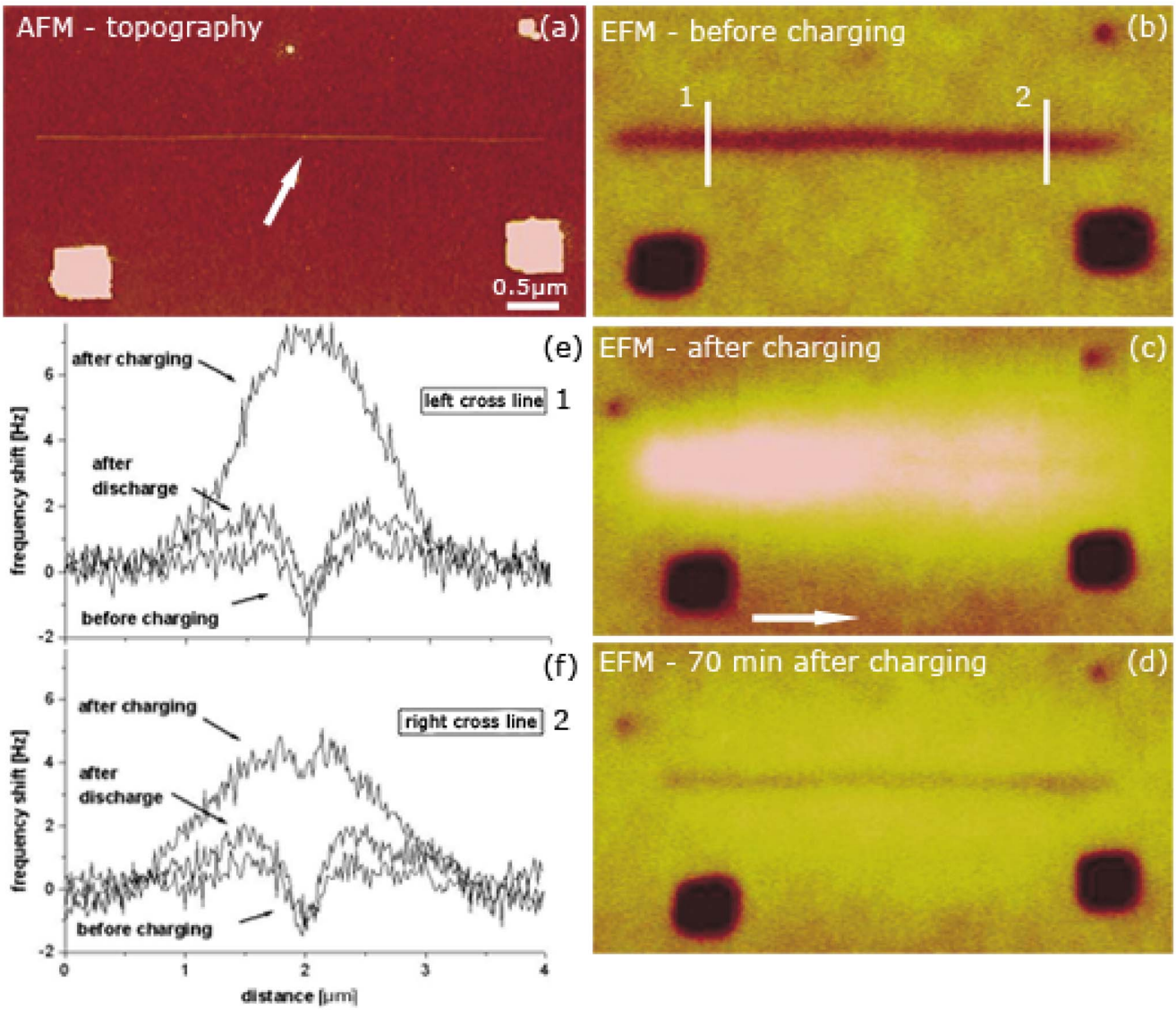

FIG. 10. (Color online) (a) AFM topography scan of a 5.5 μm long double-walled CNT of 1.5 nm diameter. Square metal markers are visible. The white arrow indicates the injection point. (b) EFM image before charging (5 Hz color scale, −1.7 Hz, V_{EFM}=−2 V). The vertical bars labeled 1 and 2 indicate two positions used for cross sections along the CNT, displayed in (e) and (f), respectively. (c) EFM picture after a charge injection using V_{inj}=−5 V for 3 min. The EFM scan has been taken from left to right, as indicated by the white arrow. The left part of the nanotube appears much brighter than right one, indicating that the nanotube gets gradually discharged during the scan acquisition. Metal markers remain uncharged throughout the scan. (d) EFM image taken 70 min after charging, showing the dark feature associated with the nanotube capacitive signal, surrounded by a faintly bright homogeneous halo. (e) Cross sections at the position labeled 1 in (b) taken before charging, after charging and 70 min after charging. (f) Same plot at the position labeled 2 in (b). The discharge of the CNT during the EFM scan shown in (c) is visible by comparison between the cross sections in (e) and (f).

ing Fig. 9(c) are shown in Figs. 9(d) and 9(e), respectively. The time between two successive EFM images is 40 min. A discharge—though not abrupt here—is evidenced by comparison of the SWCNT EFM images of Figs. 9(c) (5.6 Hz frequency shift at midscan) and 9(d) (4.1 Hz frequency shift at midscan), while no significant change is observed upon further scanning, as seen by comparison of Figs. 9(d) and 9(e), and from the following EFM scans (not shown here). We conclude that the SWCNT in Fig. 9 undergoes a continuous discharge process, in contrast with the abrupt discharge mechanisms presented in Sec. III.

We now discuss the injection experiment performed on 5.5 μm long double-walled nanotube with diameter 1.5 nm [topography scan in Fig. 10(a)]. The EFM scan prior to charging is shown in Fig. 10(b). Both the uncharged DWCNT and metal markers appear as dark features in this image. The data were taken with V_{EFM}=−2 V. The EFM scan has been performed from left to right. The vertical bars indicate the lines along which the frequency shift cross sections have been acquired at each side of the DWCNT [see Figs. 10(e) and 10(f) for the cross sections at positions 1 and 2, respectively]. Positions 1 and 2 are separated in time by 25 min in each EFM image. The charge injection was performed with the tip biased at V_{inj}=−5 V and pressed at the middle of the nanotube for 3 min. The first scan after charge injection is displayed in Fig. 10(c). The nanotube appears

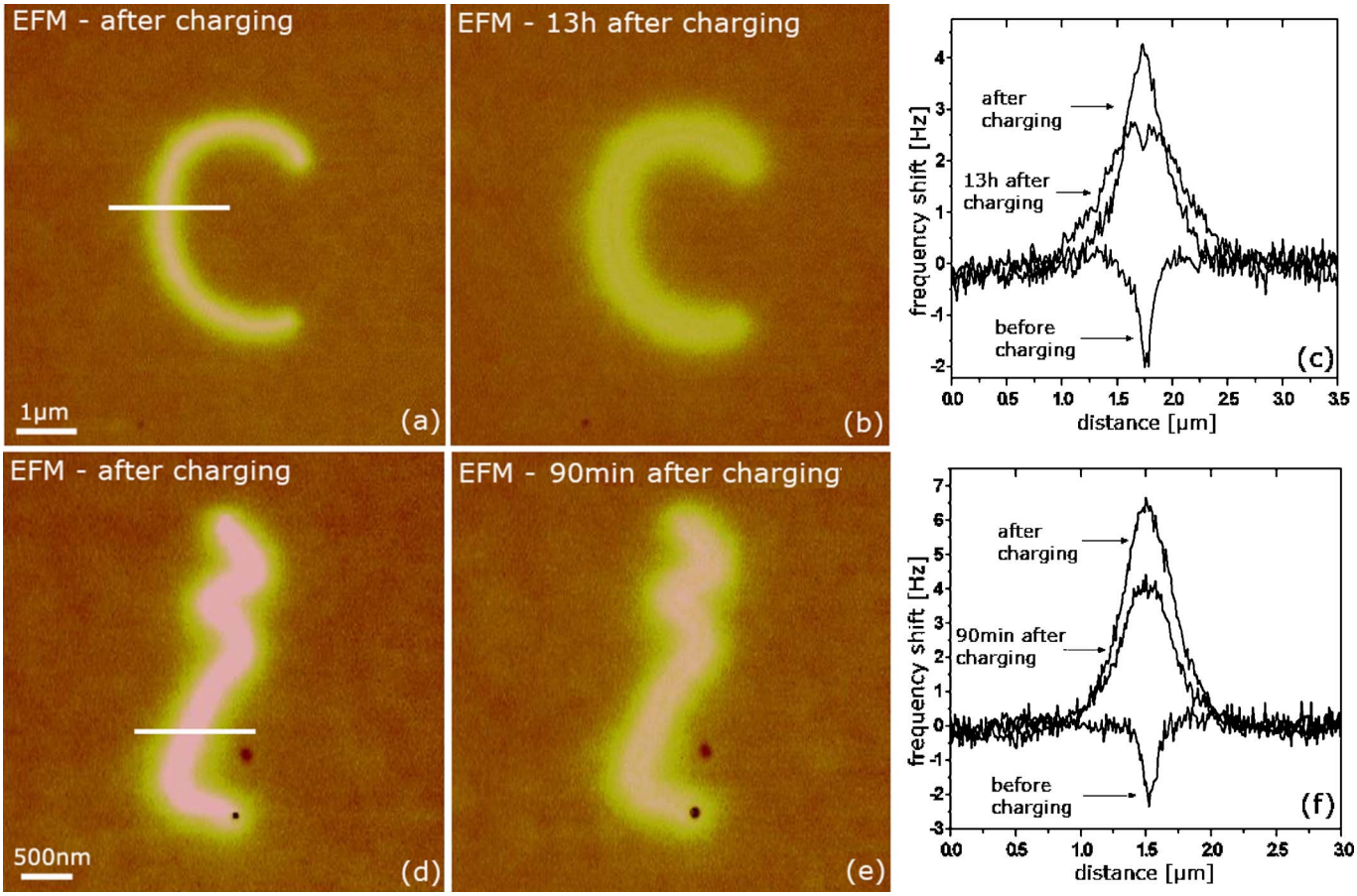

FIG. 11. (Color online) (a) EFM image (20 Hz scale, $V_{EFM}=-2$ V) of a MWCNT with 30 nm diameter after charge injection ($V_{inj}=-5$ V). The horizontal bar across the nanotube capacitive footprint indicates the place where frequency shift cross section has been taken. (b) EFM scan of the same nanotube 13 h after the injection. (c) Corresponding frequency shift cross sections, together with the data acquired prior to charging (the corresponding EFM image is not shown here). (d) EFM image (10 Hz scale, $V_{EFM}=-3$ V) of the MWCNT of Fig. 3 (19 nm of diameter) after charging ($V_{inj}=-5$ V for 2 min). (e) EFM scan of the same MWCNT taken 90 min after charge injection. (f) Frequency shift cross sections across the MWCNT prior to charging, after charging, and 90 min after charging.

bright, but a clear decrease of the charge can be observed from left to right, as confirmed by the cross sections in Figs. 10(e) and 10(f). In particular, the frequency shift dip associated with the DWCNT is visible in the right part of Fig. 10(c).

To show that this charge decay is due to the CNT discharge, an EFM scan obtained 70 min after charging is shown in Fig. 10(d). The nanotube capacitive footprint is here clearly and homogeneously visible and superimposed on a faintly bright halo. This demonstrates that Fig. 10(c) corresponds to a gradual discharge of the DWCNT with an ~20 min decay time constant, while Fig. 10(d) corresponds to the EFM image of the discharged DWCNT, together with residual surface charges corresponding to the faintly bright halo. The three consecutive charge states of the DWCNT on the oxide surface (neutral DWCNT, charged DWCNT together with oxide charges, and finally oxide charges after the DWCNT discharge) are also evidenced in the frequency shift cross sections in Figs. 10(e) and 10(f). Additionally, the square metal markers in the vicinity of the DWCNT remain unchanged in the EFM images of Figs. 10(b)–10(d) and are thus not affected by the DWCNT and oxide charging.

B. Continuous slow discharge of MWCNTs

Finally, we go back to the case of MWCNTs for which no abrupt discharge could be found. Two examples are presented in Fig. 11. First of all, a ~30 nm diameter MWCNT showing only a weak decay of the total charge signal 13 h after charge injection [see Figs. 11(a) and 11(b)]. In this case, a blurring of the MWCNT charge signal can be observed in Fig. 11(b). This is confirmed by the frequency shift cross section in Fig. 11(c), also showing the resurgence of the MWCNT capacitive frequency shift dip associated with the larger FWHM of the EFM signal 13 h after charge injection. Since the total EFM signal is approximately unchanged between Figs. 11(a) and 11(b), we assume that the observed blurring of the EFM image corresponds to a slow emission of the MWCNT charge to the oxide.

The second example is the 19 nm diameter MWCNT of Fig. 3. EFM images acquired after charging and 90 min after charge injection are shown in Figs. 11(d) and 11(e), respectively. The FWHM of the EFM signal is here unchanged, but the charge signal is weaker in Fig. 11(c) (+4.1 Hz) compared to Fig. 11(f) (+6.4 Hz), which means that the MWCNT is discharging to the EFM tip. No abrupt discharge could, how-

ever, be observed upon continuous scanning between the two scans of Figs. 11(d) and 11(e), demonstrating that the discharge is here continuous and similar to the case of the DWCNT of Fig. 10.

The estimation of decay times associated with continuous discharge processes of CNTs is ~20 min in the case of the SWCNT and DWCNT of Figs. 9 and 10 and ~100 min in the MWCNT of Figs. 11(d) and 11(e). From our experiments, we found that charge decay times increase with the CNT diameter. This is consistent with the case of the larger diameter MWCNT shown in Figs. 11(a) and 11(b) for which the charge is not emitted back to the EFM tip upon continuous scanning, but rather slowly migrates to the oxide surface. The decrease of charge decay times for smaller diameter CNTs may be related either to enhanced field effects due to the CNT curvature, or to the distribution of charge in the CNT shells in the case of MWCNTs. This study, however, falls beyond the scope of this paper.

V. CONCLUSION

We have reviewed in this paper electrostatic force microscopy and charge injection experiments performed on individually separated SWCNTs, DWCNTs, and MWCNTs deposited on thin insulating layers. Charge injection *in carbon nanotubes* is clearly evidenced from abrupt discharge processes occurring at nanotube specific points or at the nanotube caps, in which the delocalized CNT charge is field emitted back to the EFM tip. CNTs EFM images taken after abrupt discharging also reveal residual charges which are identified as emitted by the CNTs and trapped *in the oxide surface along the CNTs*. Enhanced emission patterns at the CNT caps have been studied as a function of the CNT diameter. Finally, the issue of oxide versus nanotube charging has been discussed in the case of SWCNTs, DWCNTs, and MWCNTs exhibiting continuous discharge processes.

These experiments show that field-emission phenomena play an important role in the electrostatics of individual CNTs probed by EFM and charge injection experiments, but these charges stored in nanotubes should be dissociated properly from charge emitted by CNTs into the oxide. The detailed charge storage mechanisms of SWCNTs and MWCNTs and their relation with classical electrostatics (i.e., do CNTs charge as capacitors?), however, remain to be clearly established from EFM experiments but require a truly quantitative analysis of the CNT charge states from EFM experiments.

ACKNOWLEDGMENTS

The authors thank C. Delerue, L. Wirtz, T. Heim, and A. Mayer for fruitful discussions. One of the authors (M.Z.) acknowledges partial financial support from the French Government and CEPHOMA centre of excellence. This work has been also supported in part by a PAI Grant No. POLONIUM 11600SA.

[1] T. S. Jespersen and J. Nygard, Nano Lett. **5**, 1838 (2005).
[2] M. S. Fuhrer, B. M. Kim, T. Durkop, and T. Brintliger, Nano Lett. **2**, 755 (2002).
[3] M. Bockrath, N. Markovic, A. Shepard, M. Thinkham, L. Guevich, L. Kouwenhoven, M. W. Wu, and L. L. Sohn, Nano Lett. **2**, 187 (2002).
[4] J. Heo and M. Bockrath, Nano Lett. **5**, 853 (2005).
[5] M. Paillet, P. Poncharal, and A. Zahab, Phys. Rev. Lett. **94**, 186801 (2005).
[6] M. Zdrojek, T. Melin, H. Diesinger, W. Gebicki, D. Stievenard, and L. Adamowicz, Phys. Rev. Lett. **96**, 039703 (2006); M. Paillet, P. Poncharal, and A. Zahab, *ibid.* **96**, 039704 (2006).
[7] M. Zdrojek, T. Mélin, B. Jouault, M. Wozniak, A. Huczko, W. Gebicki, D. Stiévenard, and L. Adamowicz, Appl. Phys. Lett. **86**, 213114 (2005).
[8] See www.nanocyl.com
[9] See, e.g., T. Mélin, D. Deresmes, and D. Stiévenard, Appl. Phys. Lett. **81**, 5054 (2002).
[10] T. Mélin, H. Diesinger, D. Deresmes, and D. Stiévenard, Phys. Rev. B **69**, 035321 (2004).
[11] T. Mélin, H. Diesinger, D. Deresmes, and D. Stiévenard, Phys. Rev. Lett. **92**, 166101 (2004).
[12] J. Lambert, G. Loubens, C. Guthmann, M. Saint-Jean, and T. Mélin, Phys. Rev. B **71**, 155418 (2005).
[13] The bigger CNT cap may here result also from the presence of a catalyst or amorphous carbon particle at the CNT apex, as visible for some CNTs in electron transmission microscopy.
[14] A. Buldum and J. P. Lu, Phys. Rev. Lett. **91**, 236801 (2003).
[15] J. M. Bonard, H. Kind, T. Stokli, and L.-O. Nilsson, Solid-State Electron. **45**, 893 (2001).
[16] S. Gupta, Y. Y. Wang, J. M. Garguilo, and R. J. Nemanich, Appl. Phys. Lett. **86**, 063109 (2005).
[17] X. Cui, M. Freitag, R. Martel, L. Brus, and P. Avouris, Nano Lett. **3**, 783 (2003).